ELSEVIER

Journal of Nuclear Materials 312 (2003) 236–248

journal of nuclear materials

www.elsevier.com/locate/jnucmat

A SANS investigation of the irradiation-enhanced α–α′ phases separation in 7–12 Cr martensitic steels

M.H. Mathon [a], Y. de Carlan [b], G. Geoffroy [c], X. Averty [d], A. Alamo [b], C.H. de Novion [a,*]

[a] *Laboratoire Léon Brillouin (CEA-CNRS), CEA/Saclay, Bat 563, 91191 Gif-sur-Yvette cedex, France*
[b] *Service de Recherches Métallurgiques Appliquées, CEA/Saclay, 91191 Gif-sur-Yvette cedex, France*
[c] *Laboratoire des Solides Irradiés, Ecole Polytechnique, 91128 Palaiseau cedex, France*
[d] *Service d'Etude des Matériaux Irradiés, CEA/Saclay, 91191 Gif-sur-Yvette cedex, France*

Received 2 July 2002; accepted 22 November 2002

Abstract

Five reduced activation (RA) and four conventional martensitic steels, with chromium contents ranging from 7 to 12 wt%, were investigated by small angle neutron scattering (SANS) under magnetic field after neutron irradiation (0.7–2.9 dpa between 250 and 400 °C). It was shown that when the Cr content of the b.c.c. ferritic matrix is larger than a critical threshold value (~7.2 at.% at 325 °C), the ferrite separates under neutron irradiation into two isomorphous phases, Fe-rich (α) and Cr-rich (α′). The kinetics of phase separation are much faster than under thermal aging. The quantity of precipitated α′ phase increases with the Cr content, the irradiation dose, and as the irradiation temperature is reduced. The influence of Ta and W added to the RA steels seems negligible. Cold-work pre-treatment increases slightly the coarsening of irradiation-induced precipitates in the 9Cr–1Mo (EM10) steel. In the case of the low Cr content F82H steel irradiated 2.9 dpa at 325 °C, where α′ phase does not form, a small irradiation-induced SANS intensity is detected, which is probably due to point defect clusters. The α′ precipitates contribute significantly to the irradiation-induced hardening of 9–12 wt% Cr content steels.

1. Introduction

Martensitic steels with 7–12 wt% Cr are candidates for the internal structures of future generation nuclear reactors (such as fusion or advanced high temperature reactors) or spallation sources, because of their remarkable resistance to swelling and of their adequate mechanical properties (tensile, impact and creep resistance up to 550 °C) [1]. But these materials suffer from radiation hardening and embrittlement below 400 °C, even at moderate doses (≈1 dpa). In order to promote their use, it is therefore necessary to understand the evolution of microstructure and its relationship with the degradation of mechanical properties, and to assess their structural stability during neutron irradiation or long thermal aging. At present, there is a major focus on reduced activation (RA) steels, which have been introduced as new materials that offer benefits on maintenance operations and waste management [2–4]. In the context of fusion applications, several alloying elements: molybdenum, niobium and nickel, present in commercial martensitic/ferritic steels, are restricted or prohibited; in RA steels, they are substituted by tungsten, vanadium and tantalum, which have a similar influence on the structure and the behaviour of the material, but exhibit a lower radiological impact.

It is in this context that a large programme has been undertaken at CEA to compare the behaviour under irradiation and long thermal aging of a great

* Corresponding author. Tel.: +33-1 69 08 32 82; fax: +33-1 69 08 82 61.
E-mail address: chdn@llb.saclay.cea.fr (C.H. de Novion).

0022-3115/03/$ - see front matter © 2003 Elsevier Science B.V. All rights reserved.
doi:10.1016/S0022-3115(02)01630-6

variety of conventional and RA martensitic steels, in order to optimize their performances. Previous publications in the Journal of Nuclear Materials refer to the effect of chemical composition on the physical metallurgy and mechanical behaviour of as-received materials [5], to the microstructure and mechanical properties evolution after thermal aging [6] and to preliminary results on the mechanical behaviour after irradiation [7]. Irradiation hardening (increase of tensile strength) depends of the chemical composition and metallurgical conditions of the steels, and decreases strongly as the irradiation temperature is increased. For the normalised-tempered steels, the hardening has been shown to increase with the Cr-content; no such simple correlation was found for cold-worked (CW) steels. In general, the RA variants present a better resistance to irradiation hardening compared with conventional high Cr steels [7].

As will be described below (Section 2), the small-angle neutron scattering (SANS) technique is in some specific cases more powerful than transmission electron microscopy (TEM) for studying precipitation at the nanometer scale in ferromagnetic martensitic/ferritic steels, either because of a more favourable contrast between precipitates and matrix (e.g. α–α' phase separation), or when the particles are very small (<5 nm). In addition, SANS examines a much larger volume of material than TEM.

The aim of this work was therefore to study using SANS the evolution of microstructure in RA and conventional martensitic steels after neutron irradiation, focussing on the α–α' phase separation, and to define the role of chemical composition, of irradiation conditions and of dislocation density.

The results obtained will be compared to those published recently on the thermally-aged materials [8], and will allow a preliminary analysis of the mechanical behaviour of irradiated steels.

2. Background

Numerous investigations performed since the 80s have shown that several phases precipitate in conventional martensitic/ferritic steels during irradiation between 400 and 550 °C (see review by Maziasz [9], and also Refs. [10–12]). Depending on chemical composition, these are mainly η (M_6C) carbide, G ($Mn_7Ni_{16}Si_7$) and χ ($Fe_{36}Cr_{12}Mo_{10}$) intermetallics, and Cr-enriched b.c.c. α' solid solution. These phases have been generally observed using analytic electron microscopy. On the other hand, at lower temperatures (300 °C), radiation-induced precipitation has not been found in these materials after irradiation up to 40 dpa [9]. In the case of a 9Cr-2WVTa RA steel, precipitation of tantalum initially in solution has been suggested to explain the deterioration of resistance to radiation embrittlement at high fluence and high temperature (400–450 °C) [13].

The unmixing of the ferrite below 600 °C into two isomorphous b.c.c. phases, one Fe-rich (α phase) and the other Cr-rich (α' phase), is an important feature of the binary Fe–Cr equilibrium phase diagram (see Fig. 1), where it is observed in thermally-aged alloys with Cr content between 10 and 90 at.%. The phase separation occurs at the nanometer scale and induces hardening of the binary solid solution [14]. α' has also been observed in martensitic/ferritic steels by TEM after thermal aging or irradiation at 400–550 °C for Cr content above 13 wt% [11,12]. It could be studied in some detail in a neutron-irradiated ferritic F17 steel with 17 wt% Cr, where the precipitates were greater than 10 nm in size [11]. In this material, precipitation is clearly enhanced by irradiation, the α' nucleation and growth being shifted down by about – 50 °C, compared to the out-of-pile thermal aging. Weak radiation-induced periodical variations of the chromium concentration have also been observed in a MANET steel (11 at.% Cr) after high dose dual-beam irradiation at 400–425 °C [15].

In fact, it is difficult using TEM to detect and study the α–α' phase separation, because of the very weak electron scattering contrast between Fe and Cr; for example, the total α' content deduced from TEM results in the above-quoted F17 steel thermally aged at 450 °C [11], of the order of 0.5%, is probably underestimated, as a value between 5% and 10% is expected from the phase diagram, and as confirmed by recent SANS experiments [16]. Similar difficulties arise with X-ray scattering. Furthermore, in industrial martensitic steels, the ferromagnetic

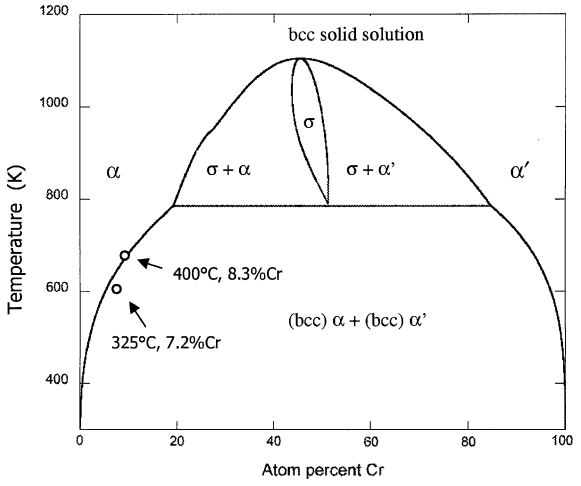

Fig. 1. Fe–Cr binary phase diagram calculated with the software 'MTDATA' from high temperature thermochemical data. Experimental points obtained in this work for the threshold of α' precipitation in industrial steels have been reported as well on the diagram.

character of the matrix and the high density of interfaces limit the possibilities for fine structural analysis by TEM. On the other hand, SANS is much more powerful to characterise the mean size, shape and number density of precipitates, because of the large difference between the neutron coherent scattering lengths of Fe and Cr (9.45×10^{-15} and 3.635×10^{-15} m respectively). Furthermore, since the ferrite is ferromagnetic, the A(q) ratio of the magnetic and nuclear SANS contrasts between matrix and particles gives information on their chemical composition [17].

α–α' phase separation has been studied in detail by SANS in thermally aged [18] or, to a lesser extent, in irradiated [19,20] binary Fe–Cr b.c.c. model alloys. The general trends of the kinetic behaviour during thermal aging of the Fe–Cr solid solution are in agreement with the assumptions of the non-linear Langer–Bar-on–Miller [21] theory of precipitation. Close to the miscibility gap boundary (i.e. for 20 at.% Cr at 500 °C, see Fig. 1), in the nucleation-growth regime of isolated α' droplets, two length scales are necessary to characterize the system: the mean distance between precipitates, and the size of precipitates [18]. SANS has also revealed the precipitation of nanosized M_2C carbides, responsible for the first stages of secondary hardening in a Fe–9Cr–1Mo alloy, particles which were too small to be detected using conventional TEM [22].

3. Experimental

3.1. Materials and specimens – irradiation conditions

The chemical compositions of the studied steels are listed in Table 1. Nine materials have been investigated:

- four RA martensitic steels, the 'LA series' from AEA-Culham, UK [2]: the LA4Ta steel with 11 wt% Cr, LA12LC and LA12TaLC with less Cr (≈8.9 wt%) and carbon (≈0.09 wt%), and which contain respectively 0.01 and 0.10 wt% Ta, and the LA13Ta steel which has a large W content (nearly 3 wt%);
- a tungsten-stabilised low Cr content RA martensitic steel of Japanese origin (supplied by JAERI): F82H (7.5Cr–2W);
- and four conventional martensitic steels: EM10 (9Cr–1Mo) and HT9 (12Cr–1Mo–0.5W) (supplied by Aubert & Duval and Sandvik respectively), T91 (9Cr–1Mo(VNb)) and MANET II (10.5Cr–0.5Mo–1Ni).

The details of the initial metallurgical states and irradiation conditions for each material are given in Table 2.

All alloys were austenitized at high temperature, then tempered at 750/800 °C. The LA materials, T91 and EM10 alloys have been 10% cold-rolled; this mechanical treatment has been shown to induce more stable impact properties after thermal aging in the case of Fe–9Cr–1Mo(V,Nb) martensitic steels [23]. In order to precise the effect of cold-work, two initial states of the EM10 alloy were irradiated: normalised and tempered (N&T) and 10% CW.

The microstructure, precipitation state and mechanical behaviour of the initial materials and their evolution after thermal aging are detailed in previous publications [5,6,8,23].

All materials except LA12TaLC were irradiated in the OSIRIS reactor at Saclay under PWR conditions (325 ± 10 °C, average doses of 0.7 and/or 2.9 dpa [1]), in the Alexandre irradiation [24]. In addition, the LA12Ta and LA12TaLC steels were irradiated in the HFR reactor (NRG, Petten) at temperatures of 250 and 400 °C for a dose of 2.4 dpa.

3.2. SANS experiments

The neutron scattering experiments were performed at the Laboratoire Léon Brillouin (CEA-CNRS), Saclay, on the PAXY small-angle instrument [25]. The wavelength λ was 0.6 nm and the sample-to-detector distance (D) was 2 m, covering a scattering vector ($\mathbf{q}$) range from 0.3 to 1.6 nm^{-1} ($q = 4\pi \sin\theta/\lambda$, where 2θ is the scattering angle). Measurements have been made at room temperature, under a saturating magnetic field $\mathbf{H}$ (=2 T) perpendicular to the incident neutron beam direction, in order to separate the magnetic and nuclear scattering cross-sections.

The samples for SANS experiments, cut and mechanically polished in the hot cells of CEA/Saclay and NRG Petten, were in the form of platelets of $5 \times 5 \times e$ mm^3, with a thickness e which has been chosen between 0.1 and 0.5 mm in order to reduce their radioactivity. The measured transmission values (≅95% for $e = 0.5$ mm and $\lambda = 0.6$ nm) showed that multiple scattering corrections were negligible.

Initial data treatment including correction, normalisation, and calibration, has been described by Cotton [26]. The analysis method used here has been reported by Mathon et al. [17,27].

In the case of ferromagnetic materials, the SANS intensity is the sum of two contributions, a nuclear and a magnetic, which depend respectively on the difference in composition and in magnetisation between particles and

[1] Recent reevaluation of effective neutron doses received by the 'Alexandre' irradiation samples in the OSIRIS reactor lead to somewhat reduced values, compared to those published previously in Refs. [7,24]: 0.7 instead of 0.8 dpa, 2.9 instead of 3.4 dpa.

Table 1
Chemical analysis of experimental steels (wt%, balance Fe, relative uncertainties = 3%)

Alloy	Cr	W	Mo	Ni	Mn	Ta	V	Si	C	N	Nb
RA-steels											
LA4Ta	11.08	0.72			0.78	0.07	0.23	0.03	0.142	0.041	
LA12LC	8.92	0.73			1.13	0.01	0.30	0.03	0.089	0.035	
LA12TaLC	8.80	0.73			1.13	0.10	0.30	0.03	0.090	0.019	
LA13Ta	8.39	2.79			0.79	0.09	0.24	0.04	0.179	0.048	
F82H	7.47	1.96		0.02	0.21	0.023	0.15	0.10	0.087	0.006	
Conventional steels											
HT9	11.8	0.51	0.99	0.48	0.50		0.29	0.37	0.21	NA[a]	<0.02
MANET II	10.37	–	0.58	0.65	0.76		0.21	0.18	0.10	0.032	0.16
T91	8.5		0.97	0.13	0.37		0.20	0.13	0.105	0.051	0.075
EM10 (N&T)[b]	8.76	<0.005	1.05	0.18[b]	0.48		0.03	0.37	0.11	0.024	<0.005
EM10 (CW)[b]	8.39	<0.005	0.99	0.54[b]	0.52		0.02	0.33	0.107	0.0175	<0.005

[a] Not analysed.
[b] The EM10 (N&T) and EM10 (CW) steels, originating from two different casts, differ by their Ni content.

Table 2
Metallurgical conditions before aging and irradiation conditions of experimental steels

Alloy	Normalisation	Tempering	Cold-work (%)	Irradiation
RA-steels				
LA4Ta	40 min – 1030 °C	1 h – 770 °C	10	0.7 dpa at 325 °C 2.9 dpa at 325 °C
LA12LC	40 min – 1030 °C	1 h – 740 °C	10	0.7 dpa at 325 °C 2.4 dpa at 250 °C 2.4 dpa at 400 °C
LA12TaLC	40 min – 1030 °C	1 h – 750 °C	10	2.4 dpa at 250 °C 2.4 dpa at 400 °C
LA13Ta	40 min – 1030 °C	1 h – 800 °C	10	0.7 dpa at 325 °C
F82H	40 min – 1040 °C	1 h – 750 °C	–	0.7 dpa at 325 °C 2.9 dpa at 325 °C
Conventional steels				
HT9	30 min – 1050 °C	2.5 h – 780 °C	–	0.7 dpa at 325 °C
MANET II	30 min – 1075 °C	2 h – 700 °C	–	0.7 dpa at 325 °C
T91	60 min – 1050 °C	1 h – 760 °C	10	0.7 dpa at 325 °C
EM10 (N&T)	30 min – 980 °C	0.5 h – 760 °C	–	0.7 dpa at 325 °C
EM10(CW)	30 min – 980 °C	0.5 h – 760 °C	10	0.7 dpa at 325 °C

the matrix. In terms of cross-section, the SANS intensity can be written as:

$$(\mathrm{d}\Sigma/\mathrm{d}\Omega)(q) \approx f_{\mathrm{p}}[\Delta\rho^2_{\mathrm{nucl}} + \Delta\rho^2_{\mathrm{mag}} \sin^2 \alpha]F^2(q,R)S(q,R),$$

where f_{p} is the precipitated atomic fraction, and $F(\mathbf{q},R)$ the form factor of the particles; $F(\mathbf{q},R)$ includes a size distribution function $h(R)$, which was usually taken as one (or the sum of several) symmetric normalized Gaussian distribution(s). $S(\mathbf{q},R)$ is the interference term between precipitates, which is not negligible for a precipitated fraction larger than 0.01; it is described by the structure factor for a liquid-like arrangement of hard spheres, calculated analytically by Ashcroft and Lekner [28] from the Percus–Yevick equation. $\Delta\rho_{\mathrm{nucl,mag}}$ are the nuclear and magnetic contrasts given by:

$$\Delta\rho_{\mathrm{nucl,mag}} = \frac{b^{\mathrm{p}}_{\mathrm{nucl,mag}}}{v^{\mathrm{p}}_{\mathrm{at}}} - \frac{b^{\mathrm{m}}_{\mathrm{nucl,mag}}}{v^{\mathrm{m}}_{\mathrm{at}}},$$

where b is the nuclear (nucl) or magnetic (mag) mean scattering length in the precipitates (p) or in the matrix (m), and $v^{\mathrm{p,m}}_{\mathrm{at}}$ is the mean atomic volume of the precipitates (p) and of the matrix (m). α is the angle between

the magnetisation of the sample and the scattering vector **q**.

As the magnetic moments are aligned parallel to the field **H**, the magnetic scattered intensity is zero in this direction and maximum in the perpendicular direction. In order to use this anisotropy, we have considered separately the scattered intensities obtained in these two directions ($\perp$ and $\parallel$ to **H**). Some information about chemical composition can be deduced from the ratio between these two quantities, called '*A* ratio'. For homogeneous particles, the *A* ratio depends on the chemical composition, magnetisation and atomic density variations between precipitates and the matrix, and is given by:

$$A = \frac{(\mathrm{d}\Sigma/\mathrm{d}\Omega)_{\perp\vec{H}}}{(\mathrm{d}\Sigma/\mathrm{d}\Omega)_{\parallel\vec{H}}} = \frac{\Delta\rho^2_{\mathrm{nucl}} + \Delta\rho^2_{\mathrm{mag}}}{\Delta\rho^2_{\mathrm{nucl}}} = 1 + \frac{\Delta\rho^2_{\mathrm{mag}}}{\Delta\rho^2_{\mathrm{nucl}}}.$$

The *A* ratio value for Cr precipitates in α-Fe matrix is equal to 2.03. To calculate *A* for α–α′ phase separation in the Fe–Cr b.c.c. solid solution, one has to take into account the variation of the average magnetic moment of the system, μ, with the Cr atomic concentration C_{Cr}: $\mu = 2.20$–$2.39\ C_{Cr}$ in Bohr magneton units [29]. The Fe–Cr phase diagram below 500 °C, where thermodynamic equilibrium is difficult or impossible to attain for kinetic reasons, has been calculated from high temperature thermochemical data (see for example Ref. [30] and Fig. 1 from the present work). Depending of different authors, the limits of the $\alpha + \alpha'$ b.c.c. miscibility gap at 325 °C have been extrapolated as $C^{\alpha}_{Cr}(325\ ^{\circ}C) = 5$ to 8 at.% and $C^{\alpha'}_{Cr}(325\ ^{\circ}C) = 95$–97 at.% respectively. The corresponding *A* ratio value is 2.09–2.13. This *A* value is only weakly composition dependent: for example, it is equal to 2.35 for α′ with the composition Cr–13Mo–8Fe–3Si in wt% measured by Gelles and Thomas [12] in HT9 steel following irradiation at 425 °C and high dose. These *A* values for α′ precipitation are much lower than for most carbides, nitrides and intermetallic particles in α matrix, e.g. $A = 3.5$ for $(Cr_{0.65}Fe_{0.35})_{23}C_6$, but higher than for vacancy clusters, for which $A = 1.4$.

4. Results

In the initial, non-irradiated state, all materials show a strong SANS signal; this is mainly due to the $M_{23}C_6$ carbide particles formed after quench and tempering, as confirmed by the *A* ratio value, which is between 3 and 4 for all the samples, at small *q* values.

After irradiation, most samples (except those with the lowest Cr content, LA13Ta and F82H, irradiated 0.8 dpa at 325 °C) show a supplementary SANS signal, mainly observed at large *q*, with a smaller *A* ratio (≈2 in most cases) than measured in the non-irradiated state; this shows that a new nanometer-sized precipitation has formed under irradiation. An example of the fit performed on this irradiation-induced signal is shown in Fig. 2. The structural information obtained from the data analysis is summarised in Table 3. Experimental results for each material are detailed below.

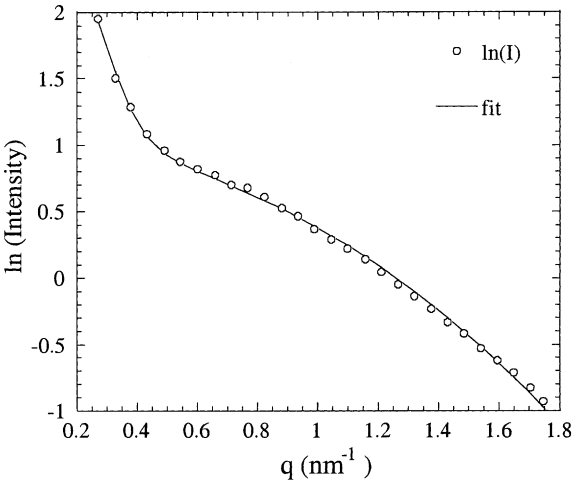

Fig. 2. Example of a data treatment performed on the LA4Ta alloy irradiated 2.9 dpa at 325 °C after subtraction of the intensity measured on the non-irradiated sample. The fit has been done assuming a gaussian size distribution of small particles with an interference contribution corresponding to a hard spheres (of radius equal to the mean radius of the precipitates) arrangement. In order to take account of the intensity at small *q* (<0.5 nm^{-1}), a second size distribution has been introduced in the fit. The precipitated fraction corresponding to this second contribution is very weak and is strongly reduced when the thermally aged (10 000 h at 350 °C) sample is used as reference.

4.1. High chromium content steels (% Cr > 10)

For Cr-rich alloys, irradiation by fast neutrons induces a large increase in the SANS intensity at $q \geqslant 0.5$ nm^{-1} (see Fig. 3).

We shall consider in detail a typical example, the behaviour of the RA steel LA4Ta (Fe–11Cr–0.7W).

In this material, as shown in Fig. 3 (open symbols), the increase in SANS signal between the sample irradiated 0.7 dpa at 325 °C and the as-received sample shows a broad maximum around $q \sim 1.1$ nm^{-1}. This behaviour indicates a spatial periodicity in the composition of the material, with a characteristic length $2\pi/q \sim 5$–6 nm, similar to that observed in the thermally aged Fe–Cr solid solution [18]. Moreover, the *A* value of the irradiation-induced SANS signal ($A = 1.9 \pm 0.2$) is in agreement with α–α′ phase separation of the ferritic matrix. The possibility of *G* or χ intermetallic phases can be discarded in LA4Ta, as they require respectively significant Ni and Mo contents. Two interpretations are possible: (1) isolated Cr-enriched α′ precipitates sur-

Table 3
Characteristics of α′ precipitates deduced from SANS data at large q (>0.5 nm^{-1})

Alloy	Total Cr content (wt%)	Metallurgical conditions	Irradiation or aging conditions	A	R (nm)	f_p	N (m^{-3})
RA-steels							
LA4Ta	11.08	N&T + CW	10 000 h – 400 °C	2.0 ± 0.2	1.5	0.0015	1.1×10^{23}
			0.7 dpa – 325 °C	1.9 ± 0.2	1.15	0.008	1.3×10^{24}
			2.9 dpa – 325 °C	2.0 ± 0.1	1.20	0.034	3.4×10^{24}
LA12LC	8.92	N&T + CW	0.7 dpa – 325 °C	1.6 ± 0.3	1.4	0.0005	5.0×10^{22}
			2.4 dpa – 250 °C	1.9 ± 0.3	1.2	0.006	6.6×10^{23}
			2.4 dpa – 400 °C	1.9 ± 0.3	0.9	0.001	3.6×10^{23}
LA12TaLC	8.80	N&T + CW	2.4 dpa – 250 °C	1.8 ± 0.2	1.25	0.0075	6.8×10^{23}
			2.4 dpa – 400 °C	ND	0.8	0.0005	1.3×10^{23}
La13Ta	8.39	N&T + CW	0.7 dpa – 325 °C	–	–	0	0
F82H	7.47	N&T	0.7 dpa – 325 °C	–	–	0	0
			2.9 dpa – 325 °C	1.2 (*)	(*)	(*)	(*)
Conventional steels							
HT9	11.8	N&T	0.7 dpa – 325 °C	3	1.2	≈ 0.008	1.0×10^{24}
MANET II	10.37	N&T	0.7 dpa – 325 °C	2.8 ± 0.3	1.2	≈ 0.003	3.1×10^{23}
T91	8.5	N&T + CW	0.7 dpa – 325 °C	1.8 ± 0.3	1.3	0.001	9.0×10^{22}
EM10	8.76	N&T	0.7 dpa – 325 °C	1.8	1.0	0.003	6.0×10^{23}
		N&T + CW	0.7 dpa – 325 °C	ND	1.5	0.002	1.4×10^{23}

ND – Not determined; (*) – Features observed at large q in F82H irradiated 2.9 dpa at 325 °C are probably vacancy clusters (see Sections 4.2 and 5.5).

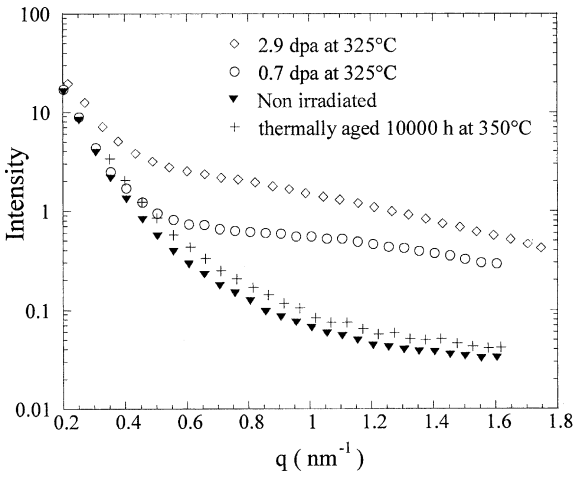

Fig. 3. Scattered intensities perpendicularly to the applied magnetic field, measured on LA4Ta samples, non-irradiated, irradiated 0.7 and 2.9 dpa at 325 °C and thermally aged 10 000 h at 350 °C.

rounded by a spherical exclusion volume depleted in Cr, or (2) a bipercolating α–α′ two-phase system, close to the image of a spinodal phase separation. Detailed work on the thermally aged Fe–Cr binary alloy suggests that for the considered Cr concentrations (<20%), the exclusion-sphere model is more adequate [18]. With this model, the best fit has been obtained considering spherical precipitates of mean radius 1.4 nm and a volume fraction equal to 0.0155. The calculation of this volume fraction is based on the assumption that only α′ precipitates (assumed of composition 95%Cr–5%Fe, as this steel does not contain Mo, see Section 3.2) contribute to the SANS intensity.

Considering the SANS results obtained in the same LA4Ta steel after thermal aging (previously published in Ref. [8]), we can observe a small increase of the scattered intensity whatever the aging duration and temperature, and in particular at 350 °C (Fig. 3), temperature close to that of irradiation. This increase, which is not compatible with a metal-diffusion governed process, given the mean displacement of Fe atoms for a duration of 10 000 h is $\approx 3 \times 10^{-11}$ m at 325 °C, cannot be associated to the precipitation of α′, but rather to a slight rearrangement of the microstructure. Consequently, in order to characterise more precisely the α–α′ phase separation, we used the sample thermally aged 10 000 h at 350 °C as the reference of the irradiated 0.7 dpa. In this case, the best fit leads to modified average radius and volume fraction of the α′ particles, 1.15 nm and 0.008 respectively, corresponding to a number density $N = 1.3 \times 10^{24}$ cm^{-3}.

On the other hand, a further increment of SANS intensity from 2000 to 10 000 h out-of-pile aging of LA4Ta is observed at higher temperature (400 °C) for $q \geqslant 0.8$ nm^{-1}, with $A = 2$; this is consistent with the

precipitation of α′ particles of mean radius 1.5 nm and a total volume fraction of 0.0015 [8]. Comparison with the data of Fig. 3 shows directly the enhancement of α–α′ phase separation by neutron irradiation.

The effect of irradiation dose is evident in the LA4Ta material: after 2.9 dpa at 325 °C, the SANS intensity is higher than after 0.7 dpa (see Fig. 3), due to an increase in α′ volume fraction. For this long irradiation, the SANS intensity is so high that the effect of the reference sample on data analysis is weak; comparable precipitate parameters have been found with the non-irradiated sample (see fit in Fig. 2) and with the thermally aged one taken as reference: $R = 1.2$ nm, close to the mean radius observed after the lowest irradiation dose (0.7 dpa), $f_p = 0.038$, and $N = 3.4 \times 10^{24}$ cm^{-3} (2–3 times larger than after 0.7 dpa).

In fact, the data on the low-Cr content F82H steel discussed below (Section 4.2) show that the contribution of point defect clusters to the SANS intensity is small, but not negligible. Considering the case of the LA4Ta alloy irradiated 2.9 dpa at 325 °C, if we assume in a first approximation that this contribution is the same than estimated for F82H irradiated in similar conditions, the precipitated α′ fraction reevaluated after correction is found slightly smaller, 0.034 (instead of 0.038) (see Section 5.5).

The two other Cr-rich materials, HT9 (Fe–12Cr–1Mo–0.5W) and MANET II (Fe–10.5Cr–0.5Mo), show also a large increase of the scattered intensity after 0.7 dpa at 325 °C, but, contrary to LA4Ta, the SANS intensity increment is a monotonically decreasing function with increasing q and shows no maximum. Also, the A ratio, close to 3 in both cases, is higher than calculated for α–α′ phase separation. Therefore, these materials probably contain another irradiation-induced precipitated phase; this could be M_6X carbonitride, which has been observed in irradiated HT9, but only above 400 °C [9,11]. The fit of the data shows the existence of two families of precipitates, with average radii of 6 and 1.2 nm respectively. Assuming that the small precipitates are α′, with a chemical composition of 95%Cr–5%Fe, we calculate the volume fractions and density numbers given in Table 3.

4.2. Low chromium content steels (% Cr < 10)

When the chromium concentration of the steel is reduced, the intensity of the radiation-induced SANS signal decreases. For a Cr content of 9 wt% (e.g. in LA12LC), only a weak effect is seen after 0.7 dpa at 325 °C. In these samples, the evidence of α–α′ unmixing could only be demonstrated by irradiation performed at lower temperature and higher dose (250 °C, 2.4 dpa). The effect of irradiation temperature is shown for LA12LC in Fig. 4, where the SANS curves are compared after irradiation at a dose of 2.4 dpa, at two

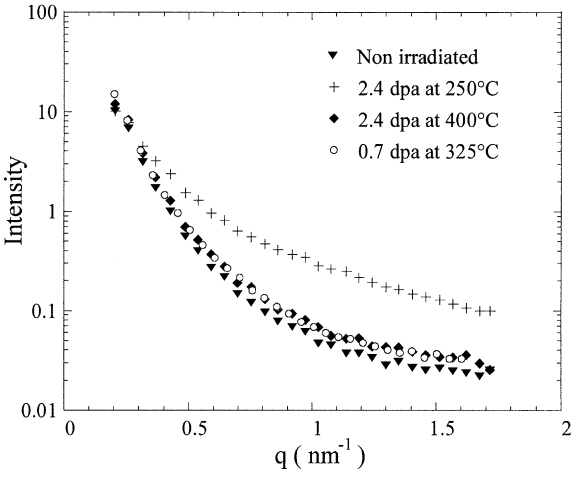

Fig. 4. Scattered intensities perpendicularly to the applied magnetic field, measured on LA12LC samples, non-irradiated and irradiated 0.7 dpa at 325 °C and 2.4 dpa at 250 and at 400 °C.

temperatures, 250 and 400 °C. For the irradiation performed at lower temperature (250 °C), one observes a marked increase in the SANS profile at large q. The A ratio value, 1.9 ± 0.3, corresponds to α′ precipitates. In order to obtain a good fit to the experimental data, it was necessary in this case to use a bimodal size distribution. The mean radii deduced from the fit are 3.2 and 1.2 nm, and the corresponding volume fractions 0.0014 and 0.006, for the large and small particles respectively. In fact, the contribution attributed to large size particles may rather be the result of a change of the precipitates (carbides) already present in the initial state; consequently, it is hazardous to consider this population as α′ precipitates. In the following, for the discussion, we shall take into account only the small size distribution. On the other hand, after 2.4 dpa at higher temperature (400 °C), the radiation-induced increase of SANS intensity is weak; the A ratio being equal to 1.9 ± 0.3, this variation can be interpreted by the formation of α′ particles ($f_p = 0.001$) with a mean radius of 0.9 nm.

For the T91 'conventional' steel (Fe–8.5Cr–1Mo) irradiated 0.7 dpa at 325 °C, the increase of SANS intensity is weak. Nevertheless, the corresponding A ratio (1.8 ± 0.3) suggests irradiation-induced α′ precipitates, with a mean radius of 1.3 nm and a volume fraction of about 0.001.

For the EM10 N&T material (Fe–9Cr–1Mo) irradiated 0.7 dpa at 325 °C, the A ratio at high q (1.8) is also in agreement with α′ precipitation. But the A ratio at low q being equal to 3, this suggests that another phase is precipitated together with α′; this might be the same one than observed after thermal aging at 400 and 450 °C ($A = 3.5 \pm 0.6$), tentatively attributed to M_2C (M = 83Cr–12Fe–5Mo in at.%) carbides [8].

For the materials with the lowest Cr content (F82H and LA13Ta), the SANS signal is unchanged by the irradiation at 325 °C up to 0.7 dpa. In the case of F82H, a weak increase in the scattered intensity is observed after 3.4 dpa at 325 °C; the A ratio value (=1.2) does not correspond to α' precipitation, but is in agreement with vacancy clusters ($A = 1.4$). These could be small cavities or dislocation loops. Assuming the simple case of spherical cavities, their average radius would be 1.1 nm, their number density 3×10^{23} m^{-3} and the corresponding volume fraction 0.002. Assuming the case of small edge dislocation loops, the analysis of the SANS data in the frame of the formalism developed by Seeger and Rühle [31] leads to an average radius of 1.05 nm and a number density of 2.2×10^{26} m^{-3}, much larger than in the case of cavities (more details will be given in a subsequent paper [16]). These numbers are discussed below in comparison to TEM results (see Section 5.5).

4.3. Influence of cold-work and of RA alloying elements

The effect of initial cold-work was considered, by comparing two samples of conventional EM10 steel (Fe–9Cr–1Mo) irradiated 0.7 dpa at 325 °C, either after 10% cold-work, or without cold-work (normalised and tempered). The difference between the two measured SANS curves was found to be weak, with a somewhat lower number of larger α' precipitates in the case of the CW material (see Table 3).

Another aim of the present study was to detect possible effects of the alloying elements Ta and W introduced in RA steels, on stability under irradiation. The effect of Ta is weak, as the SANS curves for LA12TaLC and LA12LC are very similar: a small increase after irradiation at 400 °C, and a sharper variation at 250 °C corresponding to a bimodal size distribution; the volume fractions of the small and large particles are slightly larger for LA12TaLC than for LA12LC, but within the error bars (see Section 4.2). On the other hand, no difference was observed between LA13Ta and F82H, which differ by their W content, respectively 3 and 2 wt% W; but in these samples subsequent analysis (see Section 5) shows that the Cr content remaining in the ferritic matrix is only 7 at.%, which is below the threshold value for α–α' phase separation.

5. Discussion

5.1. Effect of the Cr content on the α–α' phase separation

In order to quantify the effect of Cr content on α–α' phase separation, it is necessary to estimate the Cr concentration in the matrix, which differs from the nominal content because of the presence of Cr-rich precipitates, in particular of carbides. This was done in two ways. On the one hand, 'THERMOCALC' software [32] was directly used to calculate the phase diagram of the present steels, and showed that the equilibrium carbon concentration remaining in solid solution in the ferritic matrix after carbide precipitation during tempering ranges between 50 and 130 at. ppm. The elements entered were Fe, Cr, W, Mo, Ni, Mn, V, Si, C and N, and the software predicted in thermodynamic equilibrium at tempering temperature the presence of ferrite, $M_{23}C_6$, Laves phase and a weak fraction content of MX. On the other hand, assuming that the major precipitated phase after tempering is $M_{23}C_6$ carbides with an amount of Cr given to a first approximation by the formula $Cr_{15}M'_8C_6$, with M′ = Fe, V, W or Mo, that the average value of carbon concentration in the matrix is 100 at. ppm, and that all the precipitated carbon is in the form of $M_{23}C_6$ carbides, approximate values of the Cr concentration in solid solution in the unirradiated ferritic matrix of the various materials could be calculated. These values, which were found close to those given by THERMOCALC [8], are presented for each steel in Table 4.

Table 4 also contains, for each irradiated steel, the volume fractions of α' phase deduced from SANS analyses. The determination of the α' volume fraction depends on its chemical composition (supposed to be 95%Cr–5%Fe) and on the assumption that the irradiation-induced variation of the SANS intensity at $q \geqslant 0.5$ nm^{-1} is only due to α' precipitates. In the case of LA4Ta irradiated 2.9 dpa at 325 °C, correction has been made for the contribution of point defect clusters to the SANS intensity (see Section 5.5).

The SANS results show that the Cr-rich α' phase appears under irradiation at 325 °C in materials with a Cr concentration in the ferritic matrix equal to or larger than 8.0 at.%. The α' volume fraction deduced in the EM10 alloy seems overestimated compared to those obtained for the LA12TaLC and LA12LC alloys, of close Cr content; this is possibly due to another precipitated phase in EM10 contributing also to the scattered intensity at high q.

Except in the EM10 alloy, the volume fraction of α' measured after 0.7 dpa at 325 °C in the studied martensitic steels is found to increase monotonically with the Cr content in the matrix (Fig. 5).

At 325 °C, the Cr threshold concentration in the ferritic matrix for α–α' phase separation, calculated from the α' fraction precipitated at large dose in LA4Ta (0.034 at 2.9 dpa), when the defect cluster contribution to the SANS intensity is taken into account and assuming that the saturation is reached (see Section 5.5), is $C^{\alpha}_{Cr}(325\ °C) \approx 7.2$ at.% Cr. At 400 °C, this threshold concentration is probably close to the Cr content in the ferrite matrix of the LA12TaLC and LA12LC steels, where the precipitated α' fraction is very weak ($\approx$0.001): $C^{\alpha}_{Cr}(400\ °C) \approx 8.3$ at.% Cr. At the lowest irradiation

Table 4
Volume fraction of α' phase in the ferrite matrix of several martensitic steels after fast neutron irradiation: correlation with the total Cr content and the Cr concentration in the ferritic matrix after carbide precipitation during tempering

Alloy	Total Cr content (at.%)	Cr in matrix after tempering (at.%)	Volume fraction of α'			
			0.7 dpa at 325 °C	2.9 dpa at 325 °C	2.4 dpa at 250 °C	2.4 dpa at 400 °C
LA13Ta	9.1	7.0	0			
F82H	8.1	7.1	0	0		
T91	9.1	8.0	0.001			
EM10 N&T	9.3	8.2	$\leqslant 0.003$			
EM10 CW	9.3	8.2	$\leqslant 0.002$			
LA12TaLC	9.4	8.4			0.0075	0.0005
LA12LC	9.5	8.5	0.0005		0.006	0.001
MANET II	11.15	9.2	$\leqslant 0.003$			
LA4Ta	11.8	10.2	0.008	0.034		
HT9	12.5	10.2	$\leqslant 0.008$			

Materials are listed in the order of increasing Cr concentration in the matrix.

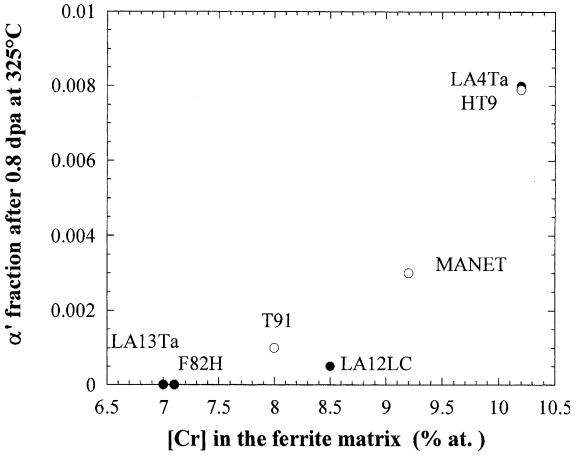

Fig. 5. α' volume fraction deduced from SANS data on 7–12Cr martensitic steels after neutron irradiation of 0.7 dpa at 325 °C as a function of the Cr amount in the ferrite matrix. Empty dots – conventional steels; full dots – RA steels. (Points obtained on the EM10 steels have not been plotted.)

temperature (250 °C), the volume fraction of α' in LA12TaLC and LA12LC, 0.006–0.0075 (weaker than the value $\sim$0.015 calculated from $C^{\alpha}_{Cr}(325\ °C) = 7.2\%$), shows that in this case saturation has not been reached at 2.4 dpa.

5.2. Mechanism of α' precipitation under irradiation

The above results show clearly that the precipitation kinetics under irradiation are much faster than during thermal aging. For the studied materials (Cr content <20 wt%), in both cases the α' phase forms by classical nucleation and growth process. Two mechanisms can be involved: either (i) a simple irradiation-accelerated mechanism, where the point defect supersaturation allows the rapid achievement of equilibrium much faster than in out-of-pile conditions at the same temperature; or (ii) an irradiation-induced mechanism, where the coupling between migrating point defects and solute atoms (Cr) can induce a non-equilibrium state, and in particular modify the composition range of existing phases.

An argument for the second mechanism is that weak binding between vacancies and Cr atoms, consistent with a solute size-effect response, has been shown experimentally in the Fe–Cr solid solution by the observation of Cr-depletion near the voids and near the grain boundaries after irradiation [19,33,34]. [2] The oversized Cr solute atoms exchange preferentially with vacancies and flow in opposite direction to vacancy flow; this will increase the local Cr concentration far from vacancy traps and therefore the tendency for α' precipitation. A recent study has also shown that coupling between fluxes of point defects and solute Cr atoms can explain in a coherent way α' precipitation kinetics under electron irradiation and under simple thermal aging in Fe-10 to 25 wt% Cr [20].

Direct evidence for the irradiation-induced mechanism could be a modification of the $\alpha + \alpha'$ miscibility gap boundary, compared to the thermodynamic equilibrium case. However, the Cr threshold concentrations in the ferrite for α' precipitation under irradiation estimated from SANS data, $C^{\alpha}_{Cr} \approx 7.2$ at.% Cr at 325 °C and 8.3 at.% Cr at 400 °C, are not significantly different from the out-of-pile values obtained from THERMO-

[2] However, the reverse behaviour, i.e. positive segregation to lath boundaries, has been observed in an irradiated commercial 12%Cr(MoVNb) martensitic steel, and was tentatively attributed to co-segregation phenomena [34].

CALC modelisations of the binary Fe–Cr equilibrium phase diagram (see Fig. 1 and Ref. [30]). Therefore, the observed difference between the irradiation and out-of-pile cases appears to be mainly of kinetic origin.

Despite the above arguments for vacancy-Cr bonding, our experimental observations are consistent with a simple irradiation-accelerated mechanism.

However, the above discussion should be taken with caution. Indeed, it has been shown experimentally, and justified theoretically from electronic structure arguments, that a chemical short-range order inversion occurs as a function of concentration in the Fe–Cr binary solid solution: from α–α' clustering for chromium contents $C_{Cr} \geqslant 10$ at.% to tendency to form an ordered compound for $C_{Cr} \leqslant 5$ at.% [35]. This strong variation of the pair potentials with composition is not taken into account in the phenomenological models such as THERMOCALC, and would argue for a steeper slope of the $\alpha + \alpha'$ miscibility gap boundary for $C_{Cr} < 10$ at.% than depicted in Fig. 1.

5.3. Influence of cold-work on α' precipitation

Cold-work pre-treatment seems to increase the coarsening kinetics of irradiation-induced precipitates in the EM10 conventional steel. A faster growth of α' precipitates in EM10 CW steels could be due either (i) to faster Cr transport due to pipe diffusion along dislocations, or (ii) to irradiation-induced Cr segregation far or close to dislocations acting as vacancy traps (depending on the sign of the chromium-vacancy interaction, see Section 5.2 and Refs. [19,33,34]), whence locally larger driving force for α' precipitation. [3]

5.4. Influence of the other alloying elements

It seems that in the RA steels (i.e. the LA series), the unique precipitated phase under irradiation is α'. But the four conventional steels which contain significant Mo and Ni contents present some departures from this simple behaviour: a larger A ratio for HT9 and MANET II, or a total precipitated fraction (for T91 and especially EM10) larger than expected from the curve depicted in Fig. 5. This could be due either to a second (unidentified) precipitated phase, or (in the case of T91 and EM10) to a role of Mo in the threshold criterion for α' precipitation.

On the other hand, the influence of other alloying elements added in the RA steels (e.g. Ta and W) was not detected. An analysis of the effect of Ta atoms would require a knowledge of their distribution between MX carbonitrides and solid solution in the ferritic matrix [8,13].

5.5. Occurrence of point defect clusters

For the weakest chromium content alloys F82H (7.47 wt% Cr) and LA13Ta (8.4 wt% Cr) irradiated respectively 0.7 and 2.9 dpa (for F82H) and 0.7 dpa (for LA13Ta) at 325 °C, the precipitation of α' phase is not observed. For the higher irradiation dose (2.9 dpa), we probably detected the formation of very small vacancy clusters in the F82H steel.

The microstructure of the W-stabilised F82H steel after neutron irradiation has been studied by TEM by several authors [37–39]. Their observations disagree in parts.

Our results concerning the absence of α' precipitation are in agreement with those of Kohno et al. [37] and Schäublin and Victoria [38]. Materna-Morris et al. [39] claimed the observation of α' in F82H irradiated 0.8 dpa at 450 and 250 °C, but this is in contradiction with other authors and ruled out by our SANS data.

Concerning vacancy clusters, Kohno et al. [37] observed cavities or He bubbles after irradiation at 365 and 405 °C, but not at temperatures greater than 550 °C. The maximum swelling occurs at 405 °C (0.14%); it is much weaker at 365 °C (0.02%). Schäublin and Victoria [38] did not observe any cavities on samples irradiated at lower temperatures (250 and 310 °C) up to 10 dpa, even after defocusing experiments in the TEM. They observed 'black dots', which in favourable cases are clearly resolved as loops when using a weak beam condition. Materna-Morris et al. [39] observed some cavities and loops after irradiation at 450 °C, but not at 250 °C.

On the basis of these TEM observations, it is likely that the defects detected by SANS (after 2.9 dpa at 325 °C) are the black dots observed by Schäublin and Victoria [38]. We have compared the defect parameters obtained from TEM observations with those deduced from our SANS data assuming either small cavities or small dislocation loops in the SANS analysis.

- By TEM on F82H irradiated 2.5 dpa at 250 °C: ϕ (defect mean size) = 4.3 nm, $N = 7.0 \times 10^{22}$ m^{-3} [38].
- By SANS on F82H irradiated 2.9 dpa at 325 °C, assuming spherical cavities: $\phi = 2.2$ nm, $N = 3.0 \times 10^{23}$ m^{-3}; assuming edge dislocation loops: $\phi = 2.1$ nm, $N = 2.2 \times 10^{26}$ m^{-3}.

Obviously, the number densities N obtained by TEM and SANS are in much better agreement if the form

[3] The larger Ni content in CW EM10 compared to the normalised-tempered material (0.54 versus 0.18 wt%, see Table 1) weakens somewhat these conclusions, as a nickel content above 0.5–0.6% has been shown to modify the precipitation state of carbides in 12Cr(MoV) steels [36].

factor of the defects is assumed to be cavity-like rather than dislocation loop-like. A reconciliation between these viewpoints might be that the majority of the black dots are very small non-collapsed vacant disks.

This defect cluster contribution to SANS probably exists in all samples after long irradiation, but is weak compared to the α' precipitates scattering when it occurs. Indeed, we have recently observed by TEM black dots and dislocation loops in the LA12LC sample irradiated 0.7 dpa at 325 °C [16]. Concerning the LA4Ta steel irradiated 2.9 dpa at 325 °C, if we take into account, in the SANS intensity analysis, a contribution of vacancy clusters equivalent to that measured in the F82H alloy, the estimated volume fraction of precipitated α' becomes equal to 0.034 (see Section 4.1). This is close to the value (0.032) calculated from the equilibrium phase diagram of Fig. 1, for complete unmixing at 325 °C of the binary solid solution $Fe_{89.8}Cr_{10.2}$ (Cr content of the ferritic matrix in LA4Ta, see Table 4) in a two-phase mixture of α and α' containing respectively 7.5 and 95 at.% Cr. Therefore, saturation of the precipitation has probably been reached in this case. New SANS analysis performed on this material after a higher irradiation dose should confirm this point.

5.6. Correlation with the evolution of mechanical properties under irradiation

First data [7] show that the radiation-induced hardening and embrittlement of the studied martensitic steels are largely determined by the irradiation temperature and vary both with the chemical composition and the metallurgical conditions of the steels (i.e. the precipitation state). In particular, all the materials irradiated in the conditions given in Table 2, whatever their Cr and α' phase contents, display a large increase ($\Delta\sigma_{irr}$) of yield stress, ranging from 100 to 275 MPa (with the only exception of LA13Ta, 0.7 dpa at 325 °C, where $\Delta\sigma_{irr} \cong 50$ MPa). No simple correlation appears between $\Delta\sigma_{irr}$ and chemical composition or microstructural parameters.

The relationship between α–α' unmixing and the mechanical properties of thermally-aged Fe–Cr binary alloys has been studied by Triki et al. [40,41] for Fe-20%Cr where the hardening is 'classical', i.e. due to dislocation-shearing of isolated coherent precipitates obtained by a nucleation-growth mechanism, which must also be the case of the presently studied martensitic steels. It was shown by these authors (and also by Park et al. [42] for the spinodally decomposed Fe–30%Cr), that the dominant mechanism to the increase of yield stress is the misfit effect (due to the coherent internal stress field), with smaller contributions from shear modulus effects and step formation at the precipitate–matrix interface ('chemical' effect). We assumed that the same hardening than in Fe–20%Cr was induced in the ferritic laths of martensitic steels by α' precipitates of similar size and volume fraction. [4] When correcting for the content of precipitated α' phase (which occurs in the yield stress increase as $f_p^{1/2}$) and for small variation in the average precipitate radius given in Table 3, the calculated α' contribution to the hardening of our steels ranges from 10–20 to 100 MPa. This is always smaller than the measured increase of yield stress, but represents a significant part of it in the case of the Cr-rich materials: for example, $\approx$60–65 MPa (calculated for an α' volume content $f_p = 0.008$) compared to measured $\Delta\sigma_{irr}$ values of 100 MPa for LA4Ta (RA steel) and 260 MPa for HT9 (conventional steel) irradiated 0.7 dpa at 325 °C. However, the main hardening contribution seems to be due to radiation-induced point defects clusters, as the largest yield stress increase at 325 °C was found in the F82H irradiated 2.9 dpa, where we observed a vacancy cluster (but no α') contribution to the SANS (see Section 5.5).

The large increase of yield stress observed for the LA12LC and LA12TaLC steels, when decreasing the irradiation temperature from 325 to 250 °C, contains very likely a contribution due to the corresponding enhancement of α' precipitated fraction reported in the present work (Fig. 4). The detailed analysis of the mechanical properties evolution in relationship with SANS data (including samples irradiated at higher dose) will be the subject of another paper.

6. Conclusion

1. The Small-Angle Neutron Scattering technique under applied magnetic field has been shown to be very powerful in the study of nanoscale precipitation in ferromagnetic martensitic steels.
2. The Cr-enriched b.c.c. α' phase has been shown to precipitate at the nanometer scale under neutron irradiation at temperatures as low as 250 °C, when the Cr content of the ferritic matrix is $\geqslant 8\%$ at.
3. The volume fraction of precipitated α' phase increases with Cr content, with the irradiation dose, and as the irradiation temperature is lowered. Up to 2.9 dpa, these parameters have only a weak influence on the average size of α' precipitates (radius $\approx$1.3 nm). The Cr threshold concentration in the ferrite for α–α' unmixing is lower than thought previously; it is estimated to be 7.2 at.% Cr at 325 °C and 8.3 at.% Cr at 400 °C.

[4] This transfer of hardening by a given precipitation microstructure from binary Fe–Cr alloys to complex steels, seems reasonable for normalised and tempered (N&T) materials, but more questionable for CW materials.

4. The precipitation kinetics under irradiation are much faster than during thermal aging. Our data are in qualitative agreement with a simple irradiation-accelerated mechanism, but do not completely exclude a more complex irradiation-induced mechanism, suggested by literature data on the binary Fe–Cr solid solution.
5. In low-Cr content alloys, the SANS signal after irradiation at a dose of 2.9 dpa suggests a small contribution due to vacancy clusters. This is probably related to the black dots observed by TEM. TEM and SANS data are in reasonable agreement if the defect form factor is assumed to be cavity-like.
6. Mo (and perhaps Ni) contained in conventional steels, could induce a secondary (unidentified) precipitation and/or play a role in α–α' phase separation. The influence of Ta and W added in the RA steels was not detected.
7. Cold-work pre-treatment increases slightly the coarsening of irradiation-induced precipitates in the EM10 conventional steel irradiated 0.7 dpa at 325 °C; this observation needs to be confirmed on other materials.
8. No simple correlation appears between the irradiation-induced hardening $\Delta\sigma_{irr}$ of the studied materials and their chemical composition or microstructural parameters. $\Delta\sigma_{irr}$ seems to be mainly due to point defect clusters, but for the Cr-rich materials a significant contribution comes from the precipitation of α' phase.

Acknowledgements

The authors would like to thank Professor Harry Bhadeshia and Mr Dominique Prior (University of Cambridge, UK) for many useful comments and a critical reading of the manuscript. We are indebted to Dr F. Bley (LPTCM, Grenoble, France) for drawing our attention on Refs. [40,41]. Dr Brigitte Beuneu (LLB) is acknowledged for valuable remarks and Dr Alain Lapp (LLB) for help in the SANS measurements.

References

[1] R.L. Klueh, D.R. Harries, ASTM Monograph 3, American Society for Testing and Materials, West Conshohocken, PA, 2001.
[2] D. Dulieu, K.W. Tupholme, G.J. Butterworth, J. Nucl. Mater. 141–143 (1986) 1097.
[3] M. Tamura, H. Hayakawa, M. Tanimura, A. Hishinuma, T. Kondo, J. Nucl. Mater. 141–143 (1986) 1067.
[4] K. Ehrlich, S.W. Cierjacks, S. Kelzenberg, A. Möslang, in: Effects of Radiation on Materials: 17th International Symposium, ASTM STP 1270, 1996, p. 1109.
[5] A. Alamo, J.C. Brachet, A. Castaing, C. Lepoittevin, F. Barcelo, J. Nucl. Mater. 258–263 (1998) 1228.
[6] Y. de Carlan, A. Alamo, M.H. Mathon, G. Geoffroy, A. Castaing, J. Nucl. Mater. 283–287 (2000) 672.
[7] A. Alamo, M. Horsten, X. Averty, E.I. Materna-Morris, M. Rieth, J.C. Brachet, J. Nucl. Mater. 283–287 (2000) 353.
[8] M.H. Mathon, Y. de Carlan, G. Geoffroy, X. Averty, C.H. de Novion, A. Alamo, in: S.T. Rosinski, M.L. Grossbeck, T.R. Allen, A.S. Kumar (Eds.), Effects of Radiation on Materials: 20th International Symposium ASTM STP 1405, American Society for Testing and Materials, West Conshohocken, PA, 2001, p. 674.
[9] P.J. Maziasz, J. Nucl. Mater. 169 (1989) 95.
[10] J.J. Kai, R.L. Klueh, J. Nucl. Mater. 230 (1996) 116.
[11] P. Dubuisson, D. Gilbon, J.L. Séran, J. Nucl. Mater. 205 (1993) 178.
[12] D.S. Gelles, L.E. Thomas, in: J.W. Davis, D.J. Michel (Eds.), Proceedings of Topical Conference on Ferritic Alloys for Use in Nuclear Energy Technologies, Metals Society of the American Institute of Mechanical Engineers, New-York, 1984, p. 559.
[13] R.L. Klueh, D.J. Alexandre, M. Rieth, J. Nucl. Mater. 273 (1999) 146.
[14] M.K. Miller, J.M. Hyde, A. Cerezo, G.D.W. Smith, Appl. Surf. Sci. 87&88 (1995) 323.
[15] N. Wanderka, E. Camus, V. Naundorf, C. Keilonat, S. Welzel, H. Wollenberger, J. Nucl. Mater. 228 (1996) 77.
[16] M.H. Mathon, C. de Novion, Y. de Carlan, G. Geoffroy, A. Alamo, in SAS 2002, XII International Conference on Small-Angle Scattering, August 25–29, 2002, Venice, Italy, to be published.
[17] M.H. Mathon, A. Barbu, F. Dunstetter, F. Maury, N. Lorenzelli, C.H. de Novion, J. Nucl. Mater. 245 (1997) 224.
[18] F. Bley, Acta Metall. Mater. 40 (1992) 1505.
[19] E.A. Little, D.A. Stowe, J. Nucl. Mater. 87 (1979) 25.
[20] V. Jaquet, PhD thesis, Ecole Polytechnique, Palaiseau, France (6 march 2000).
[21] J.S. Langer, M. Bar-on, H.D. Miller, Phys. Rev. A 11 (1975) 1417.
[22] M.H. Mathon, G. Geoffroy, Y. de Carlan, A. Alamo, C.H. de Novion, Physica B 276–278 (2000) 939.
[23] A. Alamo, J.C. Brachet, A. Castaing, C. Foucher, in: Proceedings of the Symposium on Microstructure and Mechanical Properties of Aging Materials II, The Minerals, Metals and Materials Society, 1996, p. 121.
[24] J.C. Brachet, X. Averty, P. Lamagnère, A. Alamo, F. Rozenblum, O. Raquet, J.L. Bertin, in: S.T. Rosinski, M.L. Grossbeck, T.R. Allen, A.S. Kumar (Eds.), Effects of Radiation on Materials: 20th International Symposium, ASTM STP 1405, American Society for Testing and Materials, West Conshohocken, PA, 2001, p. 500.
[25] Equipements expérimentaux, Ed. by Laboratoire Léon Brillouin, CEA Saclay, 91191 Gif-sur-Yvette, France, 1995, p. 67.
[26] J.P. Cotton, in: P. Lindner, Th. Zemb (Eds.), Neutron, X-ray and Light Scattering: Introduction for an Investigative Tool for Colloidal and Polymeric Systems, North Holland Delta Series, Amsterdam, 1991, p. 19.

[27] M.H. Mathon, C.H. de Novion, De l'intensité à la structure des matériaux, J. de Physique IV (France) 9 (1999) 127.
[28] N.W. Ashcroft, J. Lekner, Phys. Rev 145 (1966) 83.
[29] A.T. Aldred, Phys. Rev. B 14 (1976) 219;
A.T. Aldred, B.T. Rainford, J.S. Kouvel, T.J. Hicks, Phys. Rev. B 14 (1976) 228.
[30] J.O. Andersson, B. Sundman, CALPHAD 11 (1987) 83.
[31] A. Seeger, M. Rühle, Annalen der Physik 11 (1963) 216.
[32] B. Sundman, B. Jansson, J.O. Anderson, CALPHAD 9 (1985) 153.
[33] H. Takahashi, S. Ohnuki, T. Takeyama, J. Nucl. Mater. 103&104 (1981) 1415.
[34] E.A. Little, T.S. Morgan, R.G. Faulkner, Mater. Sci. Forum 97–99 (1992) 323.
[35] I. Mirebeau, M. Hennion, G. Parette, Phys. Rev. Lett. 53 (1984) 687.
[36] V. Vodarek, A. Strang, Scr. Mater. 38 (1998) 101.
[37] Y. Kohno, D.S. Gelles, A. Kohyama, M. Tamura, A. Hishinuma, J. Nucl. Mater. 191–194 (1992) 868.
[38] R. Schäublin, M. Victoria, J. Nucl. Mater. 283–287 (2000) 339.
[39] E.I. Materna-Morris, M. Rieth, K. Ehrlich, in: Effects of Radiation on Materials: 19th International Symposium, ASTM STP 1366, 2000, p. 597.
[40] A. Triki, PhD thesis, Institut National Polytechnique, Grenoble (France) (2 may 1990).
[41] A. Triki, F. Bley, Y. Brechet, F. Louchet, in: U. Messerschmidt, F. Appel, J. Heydenreich, V. Schmidt (Eds.), Electron Microscopy in Plasticity and Fracture Research of Materials, Physical Research, vol. 14, Akademie-Verlag, Berlin, 1989, p. 139.
[42] K.H. Park, J.C. LaSalle, L.H. Schwartz, M. Kato, Acta Metall. 34 (1986) 1853.